IEEE Access
Multidisciplinary | Rapid Review | Open Access Journal

Received 16 September 2023, accepted 30 September 2023, date of publication 10 October 2023,
date of current version 26 October 2023.

Digital Object Identifier 10.1109/ACCESS.2023.3323201

RESEARCH ARTICLE

Synergizing Efficient Optimal Energy Hub Design for Multiple Smart Energy System Players and Electric Vehicles

OVEIS ABEDINIA[1], (Senior Member, IEEE), AFSHAR SHORKI[2], VENERA NURMANOVA[1], AND MEHDI BAGHERI[1], (Senior Member, IEEE)

[1]Electrical and Computer Engineering Department, School of Engineering and Digital Sciences, Nazarbayev University, Astana 010000, Kazakhstan
[2]Department of Mechanical Engineering, Iran University of Science and Technology, Tehran 1684613114, Iran

Corresponding author: Mehdi Bagheri (mehdi.bagheri@nu.edu.kz)

This work was supported in part by the Faculty Development Competitive Research Grant (FDCRG), Nazarbayev University under Project 021220FD1251; and in part by the Collaborative Research Project Grant (CRP), Nazarbayev University under Project 021220CRP0322.

ABSTRACT The growth in energy consumption and pollution has led to increase the utilization of clean energy resources and electric vehicles (EVs), making the issue of network uncertainty a crucial concern. A multi-energy system offers an optimal approach to enhance the reliability, flexibility, and efficiency of an energy dispatch system through utilizing diverse energy generation resources. In this study, a new design for an optimal load distribution system, considering cost factors and CO_2 reduction, is discussed. The model includes different energy generation players, such as combined heat and power units (CHP), gas boilers, water pumps, heat storage units, hydrogen storage systems (HSS), photovoltaic arrays (PV), and wind turbines (WT), to create a broad model for analysis and examination. The model takes into account the random charging consumption of EVs and uncertainties in renewable energy generation enabling a comprehensive assessment and analysis over future energy price uncertainties. Using demand response (DR) program, electrical and thermal systems are modeled and employed, and the effects of the water pump and HSS are discussed. An improved version of particle swarm optimization (PSO) is also used to address the optimization problem. The obtained results validate the performance of the proposed approach by showcasing a synchronized charge/discharge mode for EVs, while simultaneously minimizing the total cost.

INDEX TERMS Demand response, renewable energy, electric vehicles (EVs), hydrogen storage system.

NOMENCLATURE

EVs	Electric vehicles.
CHP	Combined heat and power unit.
HSS	Hydrogen storage system.
PV	Photovoltaic array.
WT	Wind turbine.
DR	Demand response.
PEV	Plug-in EV.
RPL	Renewable penetration level.
EH	Energy hub.
SREH	Smart residential energy hub.
MES	Micro-energy system.
PD	Probability distribution.
RDERs	Renewable distributed energy resources.
DDEVs	Day-to-day driving distance of EVs.
PDF	Probability density function.
FC	Fuel cell.
DSM	Demand-side management.
EVA	EV aggregator.
PSO	Particle swarm optimization.
IPSO	Improved PSO.

The associate editor coordinating the review of this manuscript and approving it for publication was Xiaodong Liang.

I. INTRODUCTION

The electricity demand, environmental emission, water shortage, and energy source limitations have been increasing significantly over this recent century. This potentially

requires resources management in energy sector. In a broad context, both of these can potentially have adverse influences on the network; however, with careful client-side planning and utilization of energy storage resources, these methodologies can support to mitigate different issues. In this regard, the impact of integrating of plug-in EV (PEV) into the network for charging or discharging purpose is considered as a major challenge [1]. Integration of different energy sources can be taken into account in the energy hub system, that distinguished as a suitable model to obtain the local electricity demands [2]. The energy hub system is in turn a feasible solution to provide optimal energy demand management and consumption. This concept provides a new perspective over energy management through connecting various energy carriers. The energy hub can be introduced as different units that are able to perform conversion, storage, as well as district linking of different sources (make an interface among optional energy sources and client sides based on multi-energy carrier concept). A multiple power system is also a various energy sources delivery system from all different categories of energy resources, including but not limited to gas, water, district heating, and hydrogen. In a multiple power system, energy conversion among the system units along with the units' connections are feasible. Indeed, the units' connections and collaborations will be performed through a central unit called *energy hub* which can play as an interface among the clients, generating companies, and transmission system [3]. Figure 1 shows the integrated energy concept and energy hub arrangement.

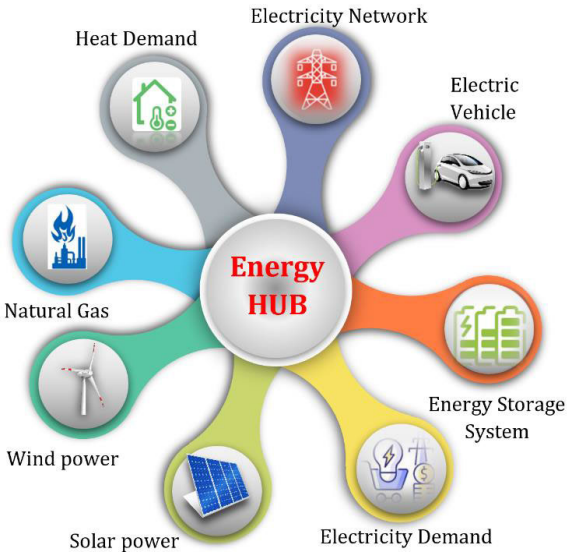

FIGURE 1. Main framework of energy hub.

In an energy system, different existing units such as electricity, natural gas along with other players are in operation independently.

In recent times, the increasing quantity and technological advancements in simultaneous energy generation have highlighted the importance of connecting energy systems. Combining various energy infrastructures, such as natural gas, heating, and cooling, can lead to enhanced energy system operation and development [4]. Several reasons drive this approach, including the ability to use energy sources on a small scale for both electricity and heating, the continuous growth in energy demand, challenges or high costs associated with replacing or expanding energy infrastructure, global efforts to reduce greenhouse gas emissions, the adoption of sustainable and environmentally friendly energy sources, and promising advancements in energy technologies, such as increased efficiency in small-scale power plants through double or triple generations [5]. Numerous research studies have previously explored load flow with multi-energy models. One of the previous research works [6] has proposed a combinatorial energy distribution framework for multiple microgrids in a combined energy organization with electrically generated heating. This framework considered various factors, including generation cost, trade cost, heating inconvenience cost, load characteristics, and electricity-consuming tools [6]. Another study proposed a real-time decentralized system considering economic dispatch limits, limited overhead transmission lines, and a self-healing approach [7]. These advanced models are operational in all sectors of electricity consumption, utility companies, and the power grid. The study demonstrated a trade-off between maximizing renewable penetration levels (RPL) in the energy hub (EH) and minimizing connected charges. To address this, a new optimal arrangement approach is proposed, allowing for adjustable RPL to be utilized in an EH for minimizing operational costs. RPL, which is determined by the network operator, can be adjusted in the scheduling plan to achieve the desired cost efficiency [8].

The micro-energy model plays a crucial role in energy consumption, where controllable energy prices can optimize micro-energy systems (MES) [9]. The ball energy model provides an overall approach for displaying MES steady-state energy equilibrium. Price-based combined demand response (DR) is explored in the context of multi-energy replacement in multi-energy connections [10]. In [10], energy management for residential users through a smart hub is modeled, considering electricity and natural gas supply for households. Physical specifications and user preferences guide energy usage approaches and control strategies. A multi-objective optimization problem is formulated for energy source allocation in the smart residential energy hub (SREH), including schedules for appliances and normal classified devices. A hybrid renewable system with wind turbines (WT), PV cells, a diesel generator, and a battery storage system is proposed in [11]. A novel technique for optimizing unit size in hybrid systems is based on the coordination between electricity generation and consumption periods, aiming for minimum cost. The electricity match rate is used for determining the optimal number of units in the hybrid system, employing a multi-objective particle swarm optimization algorithm. A study by [12] evaluates hybrid systems based on renewable energy using a multi-objective strategy with probability simulation. It employs a multi-objective genetic

algorithm, uncertainty component, and simulation module to model power systems under real operating conditions. In [13], electrical hubs are designed using a combined strategy, incorporating decision-making, multi-criteria analysis, and optimization. Criteria such as energy cost, initial investment, grid integration level, CO2 emissions, renewable energy usage, system flexibility, and load loss probability are evaluated. Reference [14] proposes a multi-objective optimum planning approach for multi-energy systems, focusing on operational economics and energy efficiency. Two types of energy storage hubs for cooling and thermal energy are considered. Reference [15] introduces a hybrid planning approach for assessing technical and economic performance in microgrids. Reference [16] offers a combined nonlinear integer programming approach for smart distributed generators, while [17] proposes a new method based on a multi-objective algorithm for determining hybrid economic and environmentally friendly load dispatching. In [18], a detailed explanation of combining singular or hybrid renewable energies in combinatorial electric and thermal systems is presented. Reference [19] introduces an optimum programming approach for a multi-energy hub system. Reference [20] discusses a thermal and electric energy management approach for a typical residential energy, considering storage systems like PHEVs and thermal reserves. However, the study examines only one EV, leaving multiple EVs in the energy hub unexplored. Reference [21] proposes a dynamic load and pollution dispatch method based on a reliable search area. The impact of an energy storage system on optimum dynamic power is analyzed, with efforts to enhance the solution through global search. Reference [22] explains a dynamic power problem considering EVs using the biography optimization algorithm. While previous literature has valuable studies, limitations are observed, including local point confinement and a lack of influential global searchers. Matching probability distribution (PD) with data uncertainty is challenging, and optimization results may not cover unconsidered scenarios, leading to vulnerability in extreme settings. Previous load flow investigations from energy hubs have shown high EV admittance, which hinders examining the impact of rising EV penetration in energy hub load. Most DR-based load flow techniques analyze only electricity DR, overlooking the evaluation of electric and thermal DR for reduced depletion cost. Furthermore, uncertainties in electricity price in energy hub load flow are not comprehensively addressed in existing literature, posing financial risk to energy hub systems. To address these inadequacies, a unique and robust strategy for societal energy hub's load flow is proposed.

(i) In this study, a new design for an optimal load distribution system is presented that considers a variety of energy resources, including CHP, gas boilers, water pumps, heat storage units, HSS, PV, and WT. The inclusion of these various energy units in a single model enables a holistic analysis and examination of the system, providing a comprehensive understanding of its performance.

(ii) This work evaluates both electric and thermal DR in the load flow analysis of the energy hub. This comprehensive approach aims to reduce the cost of energy consumption for users by considering both electric and thermal aspects, enhancing the effectiveness of DR programs.

(iii) A load flow optimization model using the locust search method is recommended to address the uncertainty surrounding the price of power, and

(iv) The suggested energy hub evaluated the large-scale random access of EVs. By incorporating these factors into the analysis, a comprehensive assessment of the economic management of EV battery charge/discharge, is provided, considering the potential impact on the overall system performance.

(v) An improved version of particle swarm optimization (PSO) is utilized by incorporating modifications and improvements tailored to the specific characteristics of our energy hub optimization problem. This enhancement ensures the convergence to better solutions and enhances the overall performance of our proposed approach.

Following, a description of energy is given, in Section II. Section III presents the goal function and associated restrictions. Suggested optimization approach through the uncertainty is discussed in Section IV. Obtained numerical analyses are provided in Section V, and finally, the conclusion is provided in Section 6.

II. THE ENERGY HUB MODEL

A. THE ENERGY HUB MODEL

The presence of energy converters throughout the energy system has been led to a significant interdependence among energy networks in several aspects. In the past, these networks utilized to operate independently of one another, with distinct infrastructures for generating, transmitting, and consuming energy at different levels; however, with the integration of energy converters, they have become interconnected, sharing similar infrastructures and functioning as a unified system. Hence, the studies of the impacts of different energy carriers on each other in the new dependent environment have received a lot of attention [23]. Figure 2 shows the input-output port layout for the energy hub. In a multi-energy system, the energy hub specifies the transformation link between the importers of input and output, which is expressed as the following connection matrix [24]:

$$\begin{bmatrix} F_1 \\ F_2 \\ \vdots \\ F_n \end{bmatrix} = \begin{bmatrix} C_{11} & C_{12} & \vdots & C_{1m} \\ C_{21} & C_{22} & \vdots & C_{2m} \\ \vdots & \vdots & \ddots & \vdots \\ C_{n1} & C_{n2} & \cdots & C_{nm} \end{bmatrix} \tag{1}$$

where, m-vector I characterizes the input energy, n-vector F characterizes the output energy flows, C is the connection

FIGURE 2. The strategy of input/output port in energy hub.

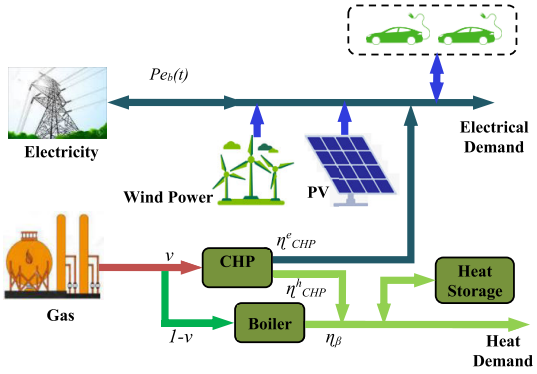

FIGURE 3. A description of the potential energy hub.

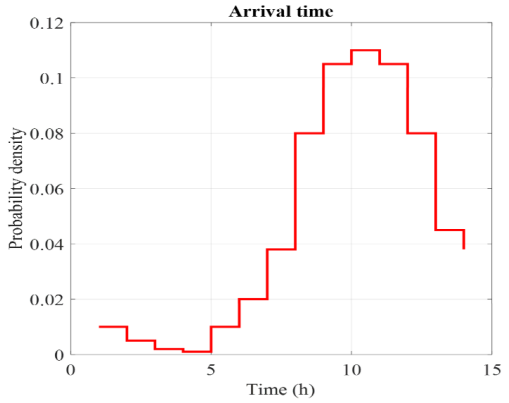

FIGURE 4. The PDs of arrival time of EVs.

matrix, and all elements of the C-matrix depicts the energy proficiency.

This study has considered the energy hub model through the energy generation, consumption, and storage units as shown in Fig. 3. The proposed renewable distributed energy resources (RDERs) are PV arrays and WTs. The power load includes basic demand and EV charging load, CHP, and RDERs. Society's surplus power can be sold wholesale to the electrical market. The plan to balance the thermal load also includes a thermal energy storage device. As illustrated in Fig. 3, the input gas is separated into 2 parts that are fed to the CHP and boiler. The transmit factor, denoted by v ($0 \leq v \leq 1$), determines the natural gas depletion distribution among the CHP and boiler.

B. ENERGY SOURCES MODELING

a: EV CHARGE

- Driving distance of EVs

The day-to-day driving distance of EVs (DDEVs) can be modeled as a function of logarithmic distribution [25], i.e., $S \sim Log - N\left(\mu_s, \sigma_s^2\right)$.

- Arrival and departures times of EVs

The owners of EVs stop charging once they leave home in the morning. The leaving time of EVs matches the normal distribution [26], where $t \sim N\left(\mu_{dep}, \sigma_{dep}^2\right)$. The holders of EVs typically start charging once they arrive home in the evening. The arrival time of EV can be displayed as a normal distribution meaning the $t \sim N\left(\mu_{arr}, \sigma_{arr}^2\right)$. The PDF in this form will be given as [26],

$$f_{arr}(t) = \begin{cases} \frac{1}{\sqrt{2\pi}\sigma_{arr}} exp\left(-\frac{(t+24-\mu_{arr})^2}{2\sigma_{arr}^2}\right) \\ \qquad 0 < t \leq \mu_{arr} - 12 \\ \frac{1}{\sqrt{2\pi}\sigma_{arr}} exp\left(-\frac{(t-\mu_{arr})^2}{2\sigma_{arr}^2}\right) \\ \qquad \mu_{arr} - 12 < t \leq 24 \end{cases} \tag{2}$$

where, $\mu_{arr} = 17.6$ and $\sigma_{dep} = 3.4$. The PDs of arrival time of EVs are depicted in Fig. 5.

- Uncoordinated charging load of EVs

In this section, the Monte Carlo approach is evaluated to model the characteristics of each EV charging load.

Next, using the characteristics of each EV load, the characteristics of the overall charging load can be obtained. To achieve sensible charging load characteristics, the simulation is carried out L times for J number of EVs. The particular stages are given as,

Phase 1: Initialize the Iteration variable l to 1.

Phase 2: Start iterating through each Electric Vehicle (EV) with variable j starting from 1.

Phase 3: Generate a random number for the charging start time of the j^{th} EV based on the Probability Density Function (PDF) of its arrival time.

Phase 4: Generate a random number for the driving distance of the j^{th} EV based on the PDF of its charging start time.

Phase 5: Analyze the charging burden of the j^{th} EV in terms of power and charging time.

Phase 6: Match the charging load characteristics of the j^{th} EV.

Phase 7: If j is less than the total number of EVs (J), increment j by 1 and go back to Phase 3. Otherwise, proceed to the next phase.

Phase 8: If the iteration variable l is less than the total number of iterations (L), increment l by 1 and go back to Phase 2. Otherwise, output the results and terminate the process.

b: THE RENEWABLE ENERGY SOURCES UNCERTAINTIES

The renewable sources in this research work are PV panels and WT. The output energy of these sources depends on the sun's irradiance, wind velocity, and specifications of the

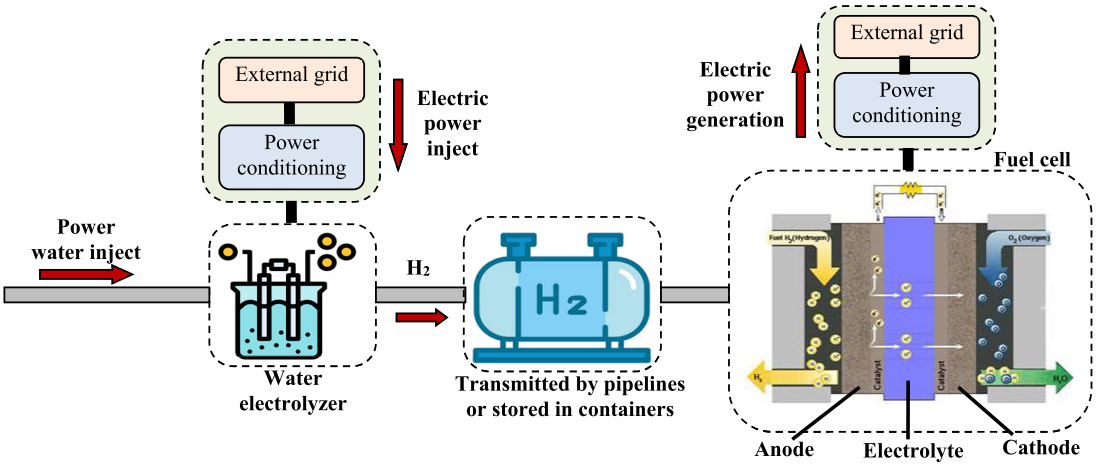

FIGURE 5. The schematics of the HSS.

associated units [25]. The first two can be calculated based on the weather forecast. The power generated by solar panels and wind turbines is stated in (3) and (4), respectively.

$$P_{PV} = f_{PV}\overline{P_{PV}}\frac{A}{A_r}[\mathbf{1} + \alpha_p(T_{PV} - T_r)] \tag{3}$$

where, f_{PV} denotes the PV output, P_{PV} denotes the nominal generated power by the PV system in a nominal condition, and A and A_r denote the forecasted and nominal amount of the irradiance, respectively. Also, a_{PV} is the coefficient of power temperature, and T_{pv} and T_r denote the actual measured and nominal temperature, respectively.

$$P_{WT} = \begin{cases} \mathbf{0}, & v \le v_{ci} \text{ or } v \ge v_{co} \\ \overline{P_{WT}}\dfrac{v - v_{ci}}{v_{co} - v_{ci}} & v_{ci} < v < v_r \\ \overline{P_{WT}}, & v_r < v < v_{co} \end{cases} \tag{4}$$

In which, V_{ci} is the wind speed, V_{co} is the cut wind speed, V_r is the nominal wind speed, V is the forecast wind speed, and P_{WT} is the output nominal power of WT.

B) Performance constraints of the electricity storage device
- Electricity storage device

$$SOC_{e,min} \le SOC(t) \le SOC_{e,max} \tag{5}$$

$$P_{WT} = \begin{cases} \mathbf{0} \le P_{char}(t) \le P_{char-max}\varpi_{BA-s} \\ \mathbf{0} \le P_{dis}(t) \le P_{dis-max}\varpi_{BA-r} \\ \varpi_{BA-s} \le \mathbf{1} \\ \varpi_{BA-r} \le \mathbf{1} \end{cases} \tag{6}$$

where, $SOC_{e;min}$ is the minimum and $SOC_{e;max}$ maximum energy in the electricity storage. ϖ_{h-st} and ϖ_{h-re} are the charge and discharge yields of the storage system. $P_{dis-max}$ and $P_{char-max}$ indicate the charge's maximum range and discharge by the electricity storage system [kW].

c: MODELING OF THE HYDROGEN STORAGE SYSTEM

The HSS plays a crucial role in enhancing the efficiency of power systems by preventing energy wastage. The HSS includes various components, such as the fuel cell (FC), storage tank, and electrolyzer, each with its specified limits. During off-peak consumption periods, surplus power is utilized to produce and store hydrogen, which is mathematically represented in (7). The constraints on electrolysis are defined in (8) and (9) for upper and lower limits, respectively. Equation (10) calculates the maximum hydrogen production achievable through the electrolysis process [20].

$$N_{H2.t}^{EL} = \frac{\eta^{EL}P_t^{EL}}{LHV_{H2}} \tag{7}$$

$$P_t^{EH} \le P_{max}^{EL} \times U_t^{EL} \tag{8}$$

$$P_t^{EH} \le P_{min}^{EL} \times U_t^{EL} \tag{9}$$

$$N_{H2.t}^{EL} \le N_{H2.max}^{EL} \times U_t^{EL} \tag{10}$$

Also, the lower and higher limits of the storage are mathematically stated in (11) and (12), respectively.

$$P_t^{H2} \ge P_{min}^{H2} \tag{11}$$

$$P_t^{H2} \le P_{max}^{h2} \tag{12}$$

Moreover, (12) imposes a limit on the initial value of the hydrogen storage.

$$P_{t0}^{H2} = P_{initital}^{H2} \tag{13}$$

The FC starts using hydrogen and generating power at peak-demand times when the available generations are insufficient to supply the demand. The limit of hydrogen usage is stated in (14). The lower and upper limits of electricity generation by the FC are shown in (15) and (16), respectively.

$$N_{H2.t}^{FC} \le N_{H2.max}^{FC} \times U_t^{FC} \tag{14}$$

$$P_t^{FC} \ge P_{min}^{FC} \times U_t^{FC} \tag{15}$$

$$P_t^{FC} \le P_{max}^{FC} \times U_t^{FC} \tag{16}$$

The hydrogen consumption by the FC is mathematically expressed in (17). The pressure inside the storage is dynamically modeled by (18). Ultimately, the limit imposed on charging at the same time and discharging of the hydrogen

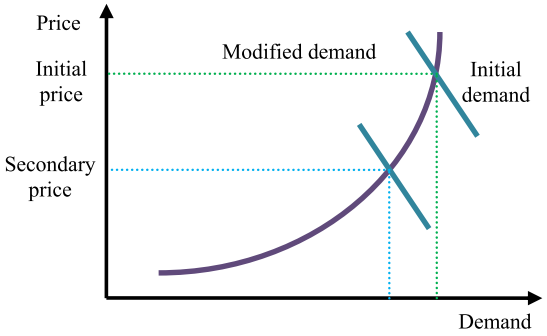

FIGURE 6. The impacts of the DSM program on the electricity price.

storage is stated by (19).

$$N_{H2.t}^{FC} = \frac{P_t^{FC}}{\eta^{FC} LHV_{H2}} \tag{17}$$

$$P_t^{H2} = p_{t-1}^{H2} + \frac{RT_{H2}}{V_{H2}} \left(N_{H2.t}^{EL} - N_{H2.t}^{FC} \right) \tag{18}$$

$$U_t^{EL} + U_t^{Fc} \leq 1 \tag{19}$$

The diagram of this procedure is illustrated in Fig. 6 for better comprehension.

- Charging limits of the plug-in electric vehicles

The plug-in electric vehicles (PEV) aggregator is fed by the main grid satisfying the charging capacity limit stated in the equation below:

$$P_{PEV.t.min} \leq P_{PEV.t} \leq P_{PEV.t.max} \tag{20}$$

In which, $P_{PEV.t.min}$ and $P_{PEV.t.max}$ are the lower/upper constrains of the PEV's charging power at time t. The limits mentioned above primarily depend on the number and capacity of aggregated PEVs and are determined using real charging data from actual PEVs. These limits are crucial for effective demand-side management (DSM) of PEVs.

DSM is a critical program within the smart grid that provides consumers with valuable information to make informed decisions about when to consume electricity, thereby minimizing their costs. It also aids in peak shaving and reshaping the demand curve. DSM enables operators to optimize the design, operation, and control of all executive actions, leading to positive impacts on power usage. Consequently, it enhances smart grid stability while reducing power costs and carbon emissions. Fig. 7 illustrates the diagram of the DSM's impact on demand and supply.

- Electricity consumption limit of the PEV

Another limit that must be added to the modeling is the amount of electricity consumption by the PEV. The power requirement for charging must be equal to the charging power capacity so that the PEVs have enough power for the daily drive. This limit is mathematically stated as follows:

$$\sum_{t=1}^{T} P_{PEV.t} + \sum_{t=1}^{T} P_{PEVload.t} = P_{PEV.total} \tag{21}$$

In which, $P_{PEV.t}$ is the PEVs' DSM at time t. $P_{PEVload.t}$ is the power requirement for uncoordinated charging power at time t, whose value is heavily dependent on the weighting parameter of PEV's required power for charging. The weighting parameter is calculated using Eq. (9). Also, $P_{PEV.total}$ denotes the overall power requirement for charging.

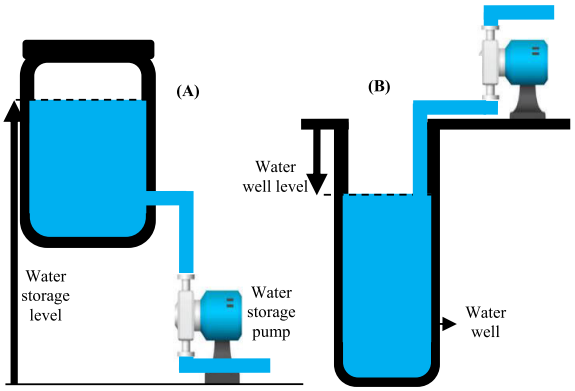

FIGURE 7. The water storage (A), the water well (B).

$$w = \frac{\sum_{t=1}^{T} P_{PEVload.t}}{P_{PEV.total}} = \frac{P_{PEV.total} - \sum_{t=1}^{T} P_{PEV.t}}{P_{PEV.total}} \tag{22}$$

The values of MDT_j, MDT_j, and P_D are determined based on the test system.

d: THE WATER SUPPLY SYSTEM

Here, the water supply system of the hub is modeled which includes a water reservoir, water well, and desalination. Fig. 8 (a) illustrate the schematics of the water reservoir and Fig. 8 (b) presents the water well.

The water reservoir and well in the hub have different power consumption patterns. The reservoir's pump consumes power during charging, while the well's pump consumes power during discharging. To ensure a balanced water supply system, the total water requirement of the hub must be equal to the sum of water obtained from the reservoir, desalination, and the well. This relationship is mathematically modeled using Eq. (23).

$$Q_t^{Dis} - Q_t^{Ch} + Q_t^{D} + Q_t^{W} = \sum\nolimits_n Load_{nt}^{W} \tag{23}$$

The water reservoir plays a vital role in improving the water supply system by reducing the energy cost through minimizing variations in power cost. The amount of water stored in the reservoir can be calculated using Eq. (24). However, there are lower and upper limits for the amount of water stored, as indicated in Eq. (25). Constraints are placed on the charge and discharge of water storage, which are expressed in Eqs (26) and (27), respectively, to ensure efficient operation. Additionally, to avoid simultaneous charging and discharging, Eq. (28) is implemented. The water volume in the well is assumed to be constant due to the significant underground water storage, and the optimization duration is limited to one

day, which is considered relatively short [12].

$$L_t^S = L_{t-1}^S - \frac{Q_t^{Ch}}{A^S} + \frac{Q_t^{Dis}}{A^S} \tag{24}$$

$$0 \le L_t^S \le Lmax^S \tag{25}$$

$$Q_t^{Ch} \le Qmax^{Ch} l_t^{Ch} \tag{26}$$

$$Q_t^{Dis} \le Qmax^{Dis} l_t^{Dis} \tag{27}$$

$$0 \le L_t^{Ch} + L_t^{Dis} \le 1 \tag{28}$$

To calculate the power used in the pump, Eq. (29) can be used which is a function of the flow of water and the water head, i.e. the height difference between the water level and the starting point for the water pump [12].

$$P^{Pump} = \frac{Q\pi g\rho}{\eta^P} \tag{29}$$

If the one-hour interval is used, Eq. (30) and (31) can be used as simplifications of the equation above [12].

$$P_t^{PW} = \frac{Q_t^W L^W g\rho}{\eta^P \psi} \tag{30}$$

$$P_t^{PS} = \frac{Q_t^{Ch}(L_t^S + L_{t-1}^S + L^G)g\rho}{2\eta^P \psi} \tag{31}$$

where, $\psi = 3.6 \times 10^6$, which is used for converting power consumed for 1 second in W unit to the power consumed in 1 hour in kW. Also, the water level is illustrated in Fig. 8.

The power used in the desalination process can be calculated using the equation below [12]. Also, the desalination device works based on reverse osmosis of seawater technology. In addition, the salinity of 35 psμ is considered for the seawater in this work.

$$P_t^D = \eta^D Q_t^D \tag{32}$$

$$0 \le Q_t^D \le Qmax^D \tag{33}$$

The total electricity consumed, given in Eq. (34), to supply the demanded water by the energy hub is composed of the power consumed by the pumps in the water well and reservoir, and the desalination process.

$$P_t^{Water} = P_t^D + P_t^{PW} + P_t^{PS} \tag{34}$$

C. OBJECTIVE FUNCTION

The fitness of the proposed model is determined by the reduction in the total cost, which comprises several components. These components include the operational cost of the energy hub relative to the network, the operating and maintenance expenses of various energy carriers, the cost associated with treating CO_2 emissions, the cost of EV battery deterioration, and the execution cost for electrical/thermal DRPs. The overall fitness of the model can be expressed as

$$min\left\{\sum_t \left(\pi_t^{buy}.P_t^{buy} - \pi_t^{sell}.P_t^{sell}\right).\Delta t + C_{OM} + C_{BAT} + C_{EM} + C_{EDR} + C_{HDR}\right\} \tag{35}$$

The CHP unit, boiler, RDERs, and thermal energy storage unit that make up the energy hub system allow us to represent the cost of operation and maintenance as follows:

$$C_{OM} = C_{OM}^{RDER} + C_{OM}^{CHP} + C_{OM}^{B} + C_{OM}^{HS} \tag{36}$$

The operation and charges of maintenance for RDERs are same as total output energy multiplied through the coefficient of unit maintenance cost [27]:

$$C_{OM}^{RDER} = \sum_T \left(P_T^{PV}.OM_{PV} + P_T^{WT}.OM_{WT}\right).\Delta t \tag{37}$$

The CHP unit operation and maintenance cost is comprised of fuel cost and price of maintenance based on the following evaluation [28]:

$$C_{OM}^{CHP} = \sum_T (G_t^{CHP}.\gamma_t^G + \left(P_t^{ECHP} + P_t^{HCHP}\right).OM_{CHP.\Delta t}) \tag{38}$$

Fuel and maintenance costs, which may be computed as follows, comprise the boiler operating and maintenance costs [28]:

$$C_{OM}^{B} = \sum_t (G_t^B.\gamma_t^G + P_t^{HB}.OM_{B.\Delta t}) \tag{39}$$

A unit maintenance cost coefficient compounds the entire thermal charge/discharge to determine the cost of thermal energy storage maintenance [28].

$$C_{OM}^{HS} = \sum_t \left(P_{dch,t}^S + P_{ch,t}^S\right).OM_{HS.\Delta t} \tag{40}$$

The cost of EV battery deterioration is taken into account to achieve the economic management of EV charge/discharge and is calculated as follows:

$$C_{BAT} = \sum_t \sum_J \left(P_{ch,j,t}^{EV} + P_{dch,j,t}^{EV}\right).\Delta t \frac{C_{R,J}^{EV}}{E_{PUTJ}^{EV}} \tag{41}$$

An environmentally conscious model is created by including the CO_2 emission treatment cost in the fitness function. The energy hub's CO_2 emission treatment costs are described as follows:

$$C_{EM} = \sum_t C_M.(P_t^{BUY}.U_{grid} + \left(P_t^{ECHP} + P_t^{HCHP}\right).U_{CHP} + P_t^{HB}.U_B).\Delta t \tag{42}$$

Applying the DR program can effectively reduce peak-load values and shift energy consumption to off-peak hours by providing incentives to consumers. This helps to decrease the load during high-price periods and increase it during low-price periods. However, modifying the main power usage pattern may cause inconvenience to consumers, which can impact their willingness to participate in the DR program. Therefore, the price of the electrical/thermal DR program must be taken into consideration. In this research, it is expected that adjusting the load in each scheduling period may cause inconvenience for the consumers. The cost of this

inconvenience is directly related to the variation in demand. This relationship is expressed as follows [29]:

$$C_{EDR} = \sum_t (\pi_{DR}^{E,down}.P_t^{p,down} + \pi_t^{E,down}.P_t^{E,up}).\Delta T \quad (43)$$

$$C_{HDR} = \sum \left(\pi_{DR}^{H,DOWN}.P_t^{H,down} + \pi_{DR}^{H,up}.P_t^{H,up}\right).\Delta T \quad (44)$$

D. OPERATIONAL LIMITS OF THE SYSTEM

- Limits of the electric DR program

The Limits of the electric DR program are as follows [30].

$$\sum_t P_t^{E,up} = \sum_t P_t^{E,down} \quad (45)$$

$$0 \le P_t^{E,up} \le MR_{UP}^{E}.P_t^{EL}.I_t^{E,down} \quad (46)$$

$$0 \le P_t^{E,down} \le MR_{down}^{E}.P_t^{EL}.I_t^{E,down} \quad (47)$$

$$0 \le I_t^{E,up} + I_t^{E,down} \le 1 \quad (48)$$

Eq (47) imposes constraints on the energy hub, requiring it to maintain power balance for all customers throughout the scheduling cycle. Eqs. (46) and (47) set limits on the maximum transmitted electric load in the upward and downward directions, respectively. The energy hub is not allowed to transmit electric load simultaneously in both directions, as specified in Eq. (48).

Limits of thermal DRP are given as follows [30]:

$$\sum_t P_t^{H,up} = \sum_t P_t^{H,down} \quad (49)$$

$$0 \le P_t^{H,up} \le MR_{up}^{H}.P_t^{HL}.I_t^{H,up} \quad (50)$$

$$0 \le P_t^{H,down} \le MR_{down}^{H}.P_t^{HL}.I_t^{H,down} \quad (51)$$

$$0 \le I_t^{H,up} + I_t^{H,down} \le 1 \quad (52)$$

Similar to the electric DRP, Eq. (49) ensures a balance between the thermal load transmitted in the upward and downward directions. The upper limits of transmitted thermal load in the upward and downward directions are stated in Eqs. (50) and (51), respectively. Eq. (52) prevents the energy hub from transmitting thermal load in both the upward and downward directions simultaneously.

- Limits of the EVs

The limits of the EVs are as follows [30].

$$E_{j,t}^{EV} = E_{j,t-1}^{EV} + P_{ch,j,t}^{EV}.\Delta t.\eta_{ch}^{EV} - \frac{P_{dch,j,t}^{EV}.\Delta t}{\eta_{dch}^{EV}} \quad (53)$$

$$E_{min,j}^{EV} \le E_{j,t}^{EV} \le E_{max,j}^{EV} \quad (54)$$

$$0 \le P_{dch,j,t}^{EV} \le P_{dch,max,j}^{EV}.Z_{j,t}^{dch} \quad (55)$$

$$z_{j,t}^{ch} + z_{j,t}^{dch} = 1, \forall j, t \in [t_{arr,j}, t_{dep,j}] \quad (56)$$

$$z_{j,t}^{ch} + z_{j,t}^{dch} = 0, \forall j, t \in [t_{arr}, t_{dep,j}] \quad (57)$$

$$0 \le \sum_J P_{ch,j,t}^{EV} \le P_{ch,max}^{EV}, 0 \le \sum_j P_{dch,j,t}^{EV} \le P_{dch,max}^{EV} \quad (58)$$

Eq (53) imposes restrictions on the batteries' ability to balance their energy. The stored energy must be kept within the Eq (54) specified range to preserve the batteries in electric vehicles. Electronic formulation restricts the maximum charge/discharge energy of EVs. These limits are stated in Eqs. (55) and (56).

$$min \left\{ \begin{array}{l} \sum_t \left(\pi_t^{buy}.P_t^{buy} - \pi_t^{sell}.P_t^{sell}\right).\Delta t\ C_{OM}\ C_{BAT} \\ +C_{EM} + C_{EDR} + C_{HDR} + MAX \left\{ \sum_T P_t^{buy}.\Delta T.\beta_T.d_t \right. \end{array} \right. \quad (59)$$

Eq (57) asserts that charging and discharging an EV is impossible once it is connected to the energy hub. According to Eq (58), EVs are neither charged nor discharged after they cannot connect to the energy hub. The combined EVs presented in this research are managed by an EV aggregator (EVA). The EVA ensures that each EV complies with the aforementioned restrictions. The transmission power between EVs and the energy hub cannot exceed a permissible stability threshold. Once the EVs have been charged and discharged, the energy hub's and EVs' maximum transmission power is constrained by (59).

- The limits of the thermal storage unit

$$H_t^S = H_{t-1}^S + P_{ch,t}^S.\Delta t.\eta_{Ch}^S - \frac{P_{dch,t}^S.\Delta t}{\eta_{dch}^S} \quad (60)$$

$$H_{min}^S \le H_t^S \le H_{max}^S \quad (61)$$

$$0 \le P_{dch,t}^S \le P_{dch,max}^S.K_t^{dch} \quad (62)$$

$$0 \le P_{dch,t}^S \le P_{dch,max}^S.K_t^{dch} \quad (63)$$

$$k_t^{Ch} + k_t^{dch} \le 1 \quad (64)$$

In Eq (60), it is stated what the thermal storage's thermal energy balance limit is. The thermal energy stored in thermal storage should be restricted between the values specified by Eq (61), much like EV batteries. Equations (62) and (63) derivative set a maximum energy charge/discharge value for the thermal storage unit. Eq. (64) ensures that the thermal storage cannot be charged and drained simultaneously [30].

- The energy balance of the energy hub

$$P_t^{buy} + P_t^{PV} + P_t^{WT} + P_t^{ECHP} + \sum_t P_{dch,j,t}^{EV} + P_t^{E,down} = p_t^{EL} + \sum_t P_{ch,j,t}^{EV} + P_t^{sell} + P_t^{E,up} \quad (65)$$

$$P_t^{HCHP} + P_t^{HB} + P_t^S + P_t^{H,down} = P_t^{HL} + P_{ch,t}^S + P_t^{H,up} \quad (66)$$

$$p_t^{HB} = G_t^B.LHV.\eta_{CHP}^e/\Delta T \quad (67)$$

$$P_t^{HCHP} = G_t^{CHP}.LHV.\eta_{CHP}^H/\Delta t \quad (68)$$

The balances among load and supply should maintain in the energy hub system for electric energy is stated by Eq. (65). Temporarily, the supplied thermal energy must be sufficient to meet the thermal demand which is stated by Eq. (66). Natural gas intake and gas-to-heat conversion efficiency are used in Eq. (67) to explain the thermal energy produced by the boiler. According to the input natural gas and effectiveness of CHP, the energy generation by CHP is evaluated by Eq. (68).

- Limits of input natural gas

The minimum and maximum amounts of natural gas input for the CHP and boiler are required. The restrictions are listed as:

$$0 \le G_t^{CHP} \le G_{max}^{CHP} \tag{69}$$
$$0 \le G_t^{B} \le G_{max}^{B} \tag{70}$$

The thermal pipe must have minimum/maximum limits for thermal power transmission.

- Limits of thermal power transmission

$$0 \le P_T^{HCHP} + P_t^{HB} + P_{dch,t}^{S} - P_{ch,t}^{S} \le P_{max}^{H} \tag{71}$$

- Limits of transmission power

The transmission power between the energy hub and grid cannot exceed the transmission limitations to ensure secure power system operation.

$$0 \le P_t^{buy} \le L_{buy}^{max} \tag{72}$$
$$0 \le P_t^{sell} \le P_{sell}^{max} \tag{73}$$

Once the obtaining power from the network, the maximum transmission energy is limited by Eq. (73) and when selling energy to the energy network, it is limited by Eq. (73).

III. PARTICLE SWARM OPTIMIZATION

A. THE CLASSIC PSO

The PSO is a metaheuristic algorithm which is utilized to solve different engineering problems for a complex problem with simplicity, robustness, and high efficiency [31]. In this algorithm, the i^{th} candidate's location vector is $x_i = \left(x_i^1, x_i^2, \ldots, x_i^D\right)$ where, D indicates the dimension and $i = 1, 2, \ldots, N$. Also, the speed vector is $v_i = \left(v_i^1, v_i^2, \ldots, v_i^D\right)$.

$$x_i^d\,(t+1) = x_i^d\,(t) + v_i^d\,(t+1) \tag{74}$$
$$v_i^d\,(t+1) = v_i^d\,(t) + C_1 \times \phi_1 \times \left(pbest_i^d\,(t) - x_i^d\,(t)\right) + C_2 \times \phi_2 \times \left(gbest^d\,(t) - x_i^d\,(t)\right) \tag{75}$$

here, $x_i^d\,(t)$ is the location and $v_i^d\,(t)$is the speed of the d^{th} element of the i^{th} candidate in the t^{th} iteration. C_1 and C_2 are the constant acceleration parameter where $C_1, C_2 \neq 0$. ϕ_1 and ϕ_2 are random values between 0 and 1. $pbest_i$, which is a set composed of $pbest_i^1, pbest_i^2, \ldots, pbest_i^d$, indicates the i^{th} candidate's best location in the t^{th} iteration. Also, $gbest^d$ indicates the best global location achieved so far from all of the candidates in the t^{th} iteration [32]. The $pbest_i$ and $gbest$ in the improved PSO (IPSO) are calculated as follows:

$$pbest_i\,(t+1) = \begin{cases} pbest_i\,(t), & O_{bj}\left(x_i\,(t+1)\right) > O_{bj}\left(pbest_i\,(t)\right) \\ x_i\,(t+1), & O_{bj}\left(x_i\,(t+1)\right) < O_{bj}\left(pbest_i\,(t)\right) \end{cases} \tag{76}$$

$$gbest\,(t) = min\left\{O_{bj}\left(pbest_1\,(t)\right), O_{bj}\left(pbest_2\,(t)\right), \ldots, O_{bj}\left(pbest_N\,(t)\right)\right\} \tag{77}$$

In which, O_{bj} is the fitness function of the candidate.

B. IMPROVED PSO

The enhancement proposed in this work includes tuning the inertia parameter, and acceleration parameter, and introducing of human interaction modeling to the algorithm which will boost the convergence speed and achieve a better solution without getting trapped in a local optimum [32]. In the enhanced version, the speeds of the candidates are updated as follows:

$$v_i^d\,(t+1) = w.v_i^d\,(t) + C_1 \times \phi_1 \times \left(pbest_i^d\,(t) - x_i^d\,(t)\right) \times \left(1 - \frac{F}{F_{max}}\right) + C_2 \times \phi_2 \times \left(lbest_i^d\,(t) - x_i^d\,(t)\right) \times \left(1 - \frac{F}{F_{max}}\right) + C_3 \times \phi_3 \times \left(Leader_i^d\,(t) - x_i^d\,(t)\right) \times e^{(1-vote_{Leader})} \tag{78}$$

$$x_i^d\,(t+1) = x_i^d\,(t) + C_4 \times \phi_4 \times v_i^d\,(t+1) \tag{79}$$

where, w is the inertia parameter, which is multiplied by the speed of the candidate in the last iteration in the first term of Eq. (78). Additionally, other modifications have been applied to the algorithm by adjusting its parameters while keeping its basic form intact. As mentioned earlier, adjusting the inertia parameter allows the algorithm to perform different types of searches. A large value of the inertia parameter puts the algorithm in global search mode, while a small value puts it in local search mode. For an optimization algorithm to perform well, it must have an adaptive inertia parameter that changes dynamically. The adaptive approach to determining the value of the inertia parameter is shown mathematically in Eq. (80), and it has been employed in [33] and [34]. In the first approach, empirical tests have been conducted where the parameter varies between 0.4 and 0.9.

$$w = \frac{1}{1 + 1.5e^{-2.6s}} \tag{80}$$

Here, s is the mutation parameter determined using Eq. (81). The starting and final values of the inertia parameter are 0.4 and 0.9, respectively.

$$s = \frac{dis_g - dis_{min}}{dis_{max} - dis_{min}} \in [0, 1] \tag{81}$$
$$dis_i = \frac{1}{N-1} \sum_{j=1, j\neq i}^{N} \sqrt{\sum_{k=1}^{D} \left(x_i^k - x_j^k\right)^2} \tag{82}$$

Here, dis_i denotes the average of distances between candidate i and other candidates which is calculated based on the Euclidian approach. dis_i, where $dis_i \in [0, 1]$, denotes the best candidate globally which is shown by dis_g. Moreover, the maximum distance, shown by dis_{max}, and minimum distance, shown by dis_{min}, are calculated based on the comparisons made among all of the dis_i's. Similar to PSO, the acceleration parameters have constant values of usually 2. When the social element C_2 is larger than the cognitive element C_1, the algorithm will be in local search mode, and when C_1 is greater than C_2, the algorithm will be in global search

mode. To achieve a more accurate optimum solution, these parameters change linearly over the iteration t as follows:

$$C_1 = C_{1i} - \left(\frac{C_{1i} - C_{1f}}{Iter_{max}}\right) \times k \tag{83}$$

$$C_2 = C_{2i} - \left(\frac{C_{2f} - C_{2i}}{Iter_{max}}\right) \times k \tag{84}$$

Here, C_{1i} C_{1f}, C_{2i}, and C_{2f} are the starting and final values of the acceleration parameters. $Iter_{max}$ denotes the maximum iteration. C_3 denotes the attraction parameters which has a value of 0.4 here. Also, C_4 is the speed scaling parameter which is 0.7 in this work. The inertia and acceleration parameters have important influences on the performance of the optimization algorithm [33]. The original PSO is improved by applying other searching methods [34]. Implementing modifications such as mutation and crossover in the PSO has increased the population diversity which can help the algorithm avoid local optima [34].

In Eq. (78), the second term consists of difference of the best location $pbest_i^d\ (t)$ and current location of the candidate $x_i^d\ (t)$ which is multiplied by $\left(1 - \frac{F}{F_{max}}\right)$ to increase the convergence speed and expected optimum point as a particle. $\frac{F}{F_{max}}$ in this term is the function assessment ratio. In this part the velocity is not improved while the distance of $pbest_i^d\ (t)$ and $x_i^d\ (t)$ are declined. The third term in Eq. (78) focuses on the local search for the best solution in which the candidates analyze their close vicinity to find the best candidate. $lbest_i^d\ (t)$ denotes the best position locally and is calculated as follows:

$$lbest_i = min\left\{O_{bj}\left(lbest_{i+1}\left(t\right)\right), O_{bj}\left(lbest_{i+2}\left(t\right)\right), \ldots, O_{bj}\left(lbest_N\left(t\right)\right)\right\} \tag{85}$$

The last term in Eq. (78) introduces the concept of voting, where candidates follow the leading candidate they have voted for to get closer to it. In each iteration, due to the superior leadership of the current leader, the opposition vote ($opVote$) is decreased, and the governance vote (goVote) is increased. This diminishes the leading ability of the opposition leader. However, if the main leader becomes stuck in a local minimum, the opposition leader takes over the lead, and the candidates follow it towards the global minimum. To control the impact of the opposition leader, $e^{(1-vote_{Leader})}$ is multiplied by the fourth term. The voting process follows the roulette wheel concept, and normalization is used to maintain asymmetric ranges of opVote and goVote between 0 and 1. To generate the initial population and allow candidates to choose their leading candidate, a preliminary biasing value is applied. The fittest candidate is chosen as the governor, and the next fittest candidate becomes the opposition. If $goVote = \varphi$, $opVote = 1 - \varphi$, where φ biases the voting. In the subsequent iterations, each candidate participates in voting ($vote_i^d$), which is a random number between 0 and 1. The leading candidate is determined as follows:

$$Leader_i^d = \begin{cases} Governor^d, & vote_i^d \le goVote \\ Opposition^d, & vote_i^d > goVote \end{cases} \tag{86}$$

After determining the leading candidate, goVote and opVote are updated. Also, the number of votes is updated using the equation below:

If $vote_i^d < goVote$

$$goVote = goVote + \frac{1}{M \times N} \tag{87}$$

Else

$$opVote = opVote + \frac{1}{M \times N} \tag{88}$$

where, M denotes the count of votes for the leading candidate. The increasing form of the voting consists of the votes given for any of the candidates. These increase votes determine which of the two leaders is the main one. The following equations are used to normalize the votes gathered after each iteration.

$$goVote = + \frac{goVote}{goVote + opVote} \tag{89}$$

$$opVote = + \frac{opVote}{opVote + goVote} \tag{90}$$

$vote_{Leader}$ in the fourth term of Eq. (78) denotes the standardized vote count expected by one of the leaders. The impact of $e^{(1-vote_{Leader})}$ in this term is explained in the following.

If $Leader_i^d = Governor_d$, then $vote_{Leader} = goVote$. Since $goVote$ is close to 1, the value of $e^{(1-vote_{Leader})}$ will incline to 1. On the other hand, if $Leader_i^d = Opposition_d$, then $vote_{Leader} = opVote$. And since $opVote$ has a very small value, $e^{(1-vote_{Leader})}$ will have a value close to e^1 or 2.3.

To update $Governor_d$ and $oppoisiton_d$, the equation below is used.

$$oppoisiton_d = \begin{cases} Governor_d, & rand_d \ge \frac{1}{N} \\ \phi \times (X_{max} - X_{min}) + X_{min}, & rand_d < \frac{1}{N} \end{cases} \tag{91}$$

$$Governor_d = gbest_d \tag{92}$$

Here, ϕ and $rand_d$ are randomly chosen numbers between 0 and 1. $d = 1, 2, \ldots, D$ represents the dimension. $oppoisiton_d$ is randomly chosen from a uniformly distributed space between X_{min} and X_{max}, otherwise, it is taken from the fittest candidate.

IV. NUMERICAL RESULTS AND ANALYSIS

A. DATA OF INPUT AND SIMULATION SETTINGS

The planning horizon is set for 1 day, and it is divided into 24 one-hour intervals. The considered energy hub system involves 300 electric vehicles (EVs), and the specifications of the EV batteries are evaluated to efficiently simulate and plan the charging. The charging energy for the EVs follows the daily load curve. The basic parameters of the EVs are

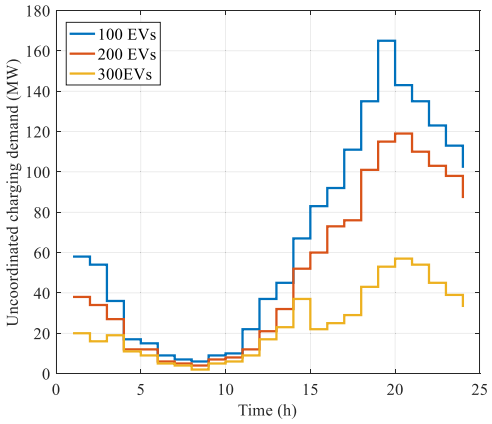

FIGURE 8. The EVs uncoordinated charging demand.

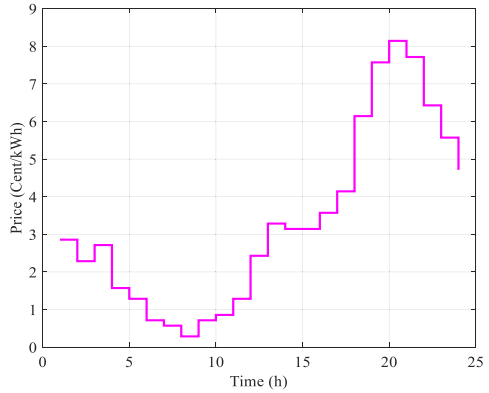

FIGURE 9. The predicted price of energy's lower limit.

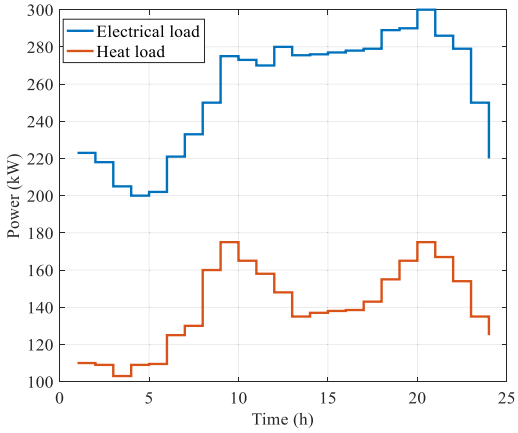

FIGURE 10. Thermal and electrical load.

presented in Table 1 [25]. Fig. 9 illustrates the uncoordinated charging demand for different numbers of EVs. The real-time electricity prices vary within the specified price bounds. The lower bound of the projected energy price is shown in Fig. 10. The parameter dt represents the highest price uncertainty, estimated to be 20% of the predicted price's lower bound.

This parameter can be obtained based on available technologies, but its value can be adjusted based on actual forecasted outcomes in practice. The selling price of surplus electricity to the grid is expected to be 10% lower than the corresponding lower bound of electricity price.

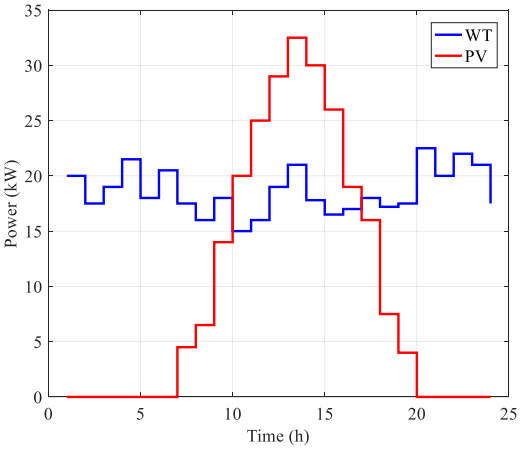

FIGURE 11. The output energy profile of PV and WT.

TABLE 1. The variables of the used EVs [24].

Category	Value
Max. size (kWh)	1000
Preliminary storage (kWh)	600
The discharging max. power (kW)	150
The stored heat energy lower/upper (kWh)	100/1000
Power charging max. size (kW)	150
Efficiency of charging	0.9

TABLE 2. The thermal energy storage parameters.

Category	Value
Max. size (kWh)	1000
Preliminary storage (kWh)	600
Efficiency of charging	0.9
The discharging max. power (kW)	150
Power charging max. size (kW)	150
The stored heat energy lower/upper (kWh)	100/1000
Efficiency of discharging	0.9

Fig. 11 displays the electrical and thermal load (excluding EV charging) profiles. Fig. 12 shows the output energy characteristics of PV and wind turbine (WT) sources [35], [36]. Additionally, Table 2 presents factors related to thermal energy storage, while Table 3 lists additional simulation variables [29], [35], [36].

B. ANALYSIS AND DISCUSSION

In order to analyze the effects of the coordinated charge/discharge method of DR and EVs through planning outcomes, three different scenarios have been considered. In every planned scenario, the pricing ambiguities have been assessed. The 3-forms of planning scenarios defined as:

Planning scenario 1: A simple planning scenario, where the EVs are in uncoordinated charge mode, is considered to show how effectively EVs' coordinated charge/discharge mode affects the total pricing.

Planning scenario 2: in comparison to planning scenario 1, the EVs will be in coordinated charge/discharge mode in this situation.

Planning scenario 3: in this planning scenario, to show the efficiency of the DR, the EVs will be in coordinated

TABLE 3. Remaining considered variables in simulation.

Variable	Unit	Value	Variable	Unit	Value
$OMCHP$	cent/kWh	2.0	$MR_{\text{up}}^{\text{H}}$	-	0.500
OM_{WT}	cent/kWh	0	$MR_{down}{}^{E}$	-	0.200
OM_{PV}	cent/kWh	0.0	$MR_{up}{}^{E}$	-	0.500
OM_{HS}	cent/kWh	0.5	λ_{t}^{G}	cent/m^3	22.00
OM_{B}	cent/kWh	2.7	$MR_{down}{}^{H}$	-	0.200
u_{CHP}	kg/kWh	0.177	LHV	kWh/m^3	9.70
u_{B}	kg/kWh	0.177	η_{CHP}^{e}	-	0.35
u_{grid}	kg/kWh	0.187	C_{tre}	cent/kg	3.36
$\pi_{DR}^{E,down}$	cent/kWh	0.10	η_{B}	-	0.8
$\pi_{DR}^{E,up}$	cent/kWh	0.10	η_{CHP}^{h}	-	0.45
$\pi_{DR}^{H,down}$	cent/kWh	0.10	G_{max}^{B}	m^3/h	100
$\pi_{DR}^{H,up}$	cent/kWh	0.10	G_{max}^{CHP}	m^3/h	100

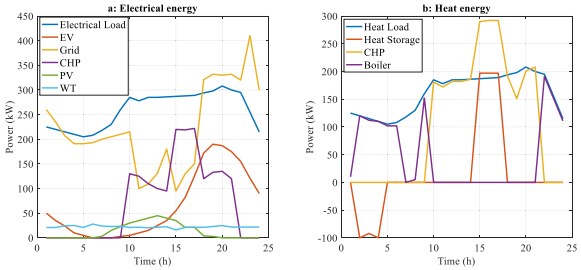

FIGURE 12. The result of power transmission under planning scenario 1.

charge/discharge mode. In addition, the DR programs are considered.

1) TRANSMISSION ANALYSIS AND COMPARATIVE OUTCOMES

The results of thermal and electrical energy transmission under planning scenario 1 are shown in Fig. 13.

In Fig. 13 (a), it can be observed that the EVs' charging demand is integrated under uncoordinated charging mode, as the EV owners start charging once they reach their destination at sunset. The CHP produces electricity during high-price periods (9-20 h) to reduce the overall energy consumption cost. As depicted in Fig. 13 (b), the CHP also generates heat during high electricity price periods. Consequently, the boiler generates heat during low-energy-cost periods (20-24 h and 5-10 h) to lower the cost of thermal energy consumption. Additionally, the heat storage unit plays a role in load planning under scenario 1. The excess heat generated by the CHP is used to charge the heat storage unit during 15-18 h. On days with negative values, the heat storage unit is discharged, as indicated in Fig. 13 (b).

Figure 14 displays the thermal and electrical energy transport outcomes under Planning Scenario 2. The coordinated charge/discharge and the shifting of EV charging requirements from high-electricity-price times to low-electricity-price ones will be observed. This is due to the fact that

TABLE 4. The comparisons of the price of various planning scenarios.

	Scenario 1	Scenario 2	Scenario 3
Total price ($)	632.2510	590.3230	556.3410

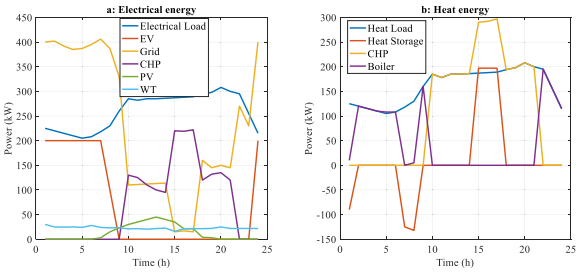

FIGURE 13. The result of transmission under planning scenario 2.

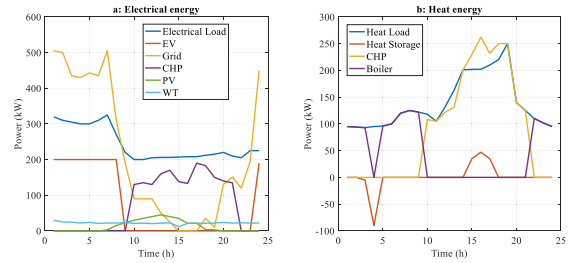

FIGURE 14. The result of transmission under planning scenario 3.

the modification in the load charging of EVs will lead to a reduction in the cost of electricity consumption. As can be seen, the EVs aren't charges in Fig. 14 (a) in every stage, due to the degradation cost of EV units is high, and the discharged power from the EVs should be purchased back by the EV owner to provide the energy needed to drive, and the electricity selling condition to the network or obtaining power to meet the demand increases the battery degradation price for the EV holders.

Fig. 15 shows the outcomes of thermal and electrical energy transfer under planning scenario 3. It is clear from comparing the actual execution of the electrical and thermal DR programs to planned scenarios 1 and 2 that the thermal and electrical load requirements have altered. Fig. 15 presents the loads earlier and later executing the thermal and electrical DR program.

After execution of the thermal/electrical DR, the load of the energy hub has moved from high-energy-cost aeras (9-21 h) to low-energy-cost periods for decreasing the price of buying energy from the network.

In response to high energy prices, the energy hub increases the energy output of the CHP to lower the purchasing cost of electricity. Since the CHP can simultaneously produce thermal and electrical energy, when the electrical energy output is increased during high-energy-cost periods, the thermal energy output also increases as a byproduct. After applying DR, the total thermal load is increased during times of high energy costs (13-19 h) to utilize the increased thermal energy output effectively. Table 4 presents pricing comparisons for several planning scenarios. Scenario 2 shows a 12% reduction

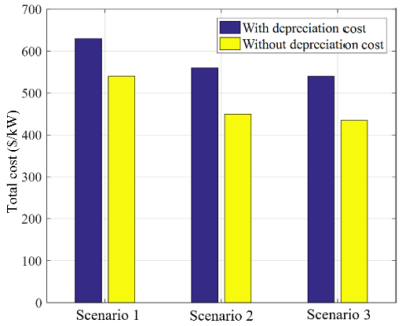

FIGURE 15. The overall cost under various scenarios including/excluding the EV degradation cost.

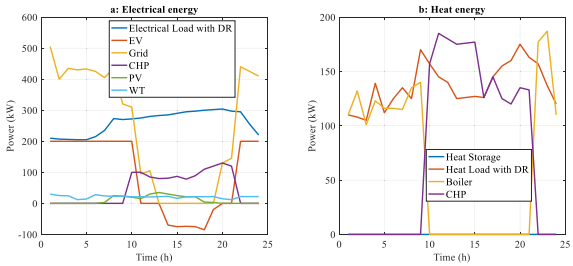

FIGURE 16. The planning outcomes in planning scenario 2 excluding the degradation cost of EVs.

in overall cost compared to scenario 1, indicating that coordinated charging and discharging of EVs successfully reduce the electricity cost for customers. Furthermore, scenario 3 has a lower overall cost than scenario 2, with a reduction of 5.76%. This demonstrates that implementing the DR program can help customers lower their overall costs by shifting their loads intelligently.

2) THE IMPACT OF EV DEGRADATION

According to the high degradation cost of EV units, EV holders are unwilling to discharge their EVs so as to increase the lifespan of their EV batteries. Hence, the EV degradation cost has a critical impact on the planning outcomes. This part presents the effects of EV degradation. The overall costs under various scenarios including/excluding EV degradation cost are depicted in Fig. 16. It can be seen in this figure that the overall cost of the scenario without considering the EV degradation is significantly lower than the scenario considering EV degradation cost which suggests that the EV degradation cost is not negligible.

The planning outcomes of scenarios 2 and 3, where EVs are in synchronized charge/discharge mode, are considered as examples. Fig. 17 displays the transmission results in scenario 2 without accounting for the cost of EV depreciation. In this case, the results show that the EVs are charged during low-energy-cost times and discharged during high-energy-cost times (13-20 h) to reduce the quantity of power purchased when the cost is high. The negative values in Fig. 17 represent the EVs being discharged during high-energy-cost periods. Fig. 16 presents the outcomes of transmission in scenario 2, excluding the EV degradation cost. Similar to the previous

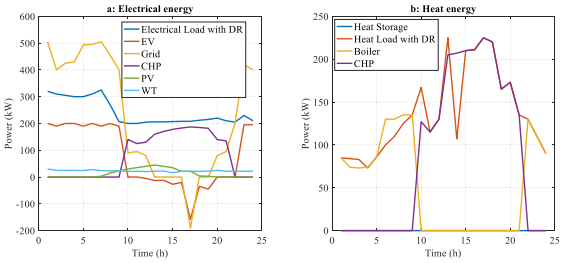

FIGURE 17. The planning outcomes in planning scenario 3 excluding the degradation cost of EVs.

TABLE 5. The CEC 2020 test function results (for D=20).

Benchmark	D=20				
	Best	Worst	Median	Mean	SD
f_1	0.00E+00	0.00E+00	0.00E+00	0.00E+00	0.00E+00
f_2	0.00E+00	2.13E-01	1.14E-01	1.31E-02	1.21E-01
f_3	1.01E+01	1.04E+00	2.00E+00	1.00E+00	1.00E+00
f_4	3.42E-02	2.14E-01	1.13E-01	2.42E-02	2.43E-01
f_5	2.11E-02	2.53E-01	2.22E-00	1.14E-02	2.55E+01
f_6	2.42E-02	3.11E-01	2.23E-01	2.53E-02	2.43E-01
f_7	2.13E-02	2.33E+00	2.53E+00	1.43E-01	1.24E+00
f_8	2.64E+00	2.42E+01	2.22E+01	3.53E+00	2.53E+00
f_9	0.00E+00	1.11E+01	1.35E+01	2.21E+01	2.11E+00
f_{10}	3.11E+01	2.53E+02	2.14E+01	1.12E+02	2.14E+01

TABLE 6. Obtained results for Wilcoxon signed-rank test.

D	Models	R+	R-	P value	+	≈	-	Dec.
20	Proposed vs GA	41	1	**0.015**	7	1	0	+
	Proposed vs PSO	40	2	**0.012**	7	1	0	+
	Proposed vs ABC	42	0	**0.014**	8	2	1	+
	Proposed vs GSA	41	1	**0.013**	7	2	1	+

results, the EVs are charged during low-energy-cost periods (22-24 h and 1-10 h) and discharged during high-energy-cost periods (12-20 h) to minimize the electricity consumption cost during peak hours.

Additionally, the energy hub sells excess energy to the network to gain profit during high-energy-cost periods (18 h). It can be inferred that without considering the EV degradation cost, the EVs are charged and discharged constantly to reduce the overall cost of the energy system. With the rapid improvement of EV batteries and decreased battery cost, EVs are expected to play an increasingly critical role in the system energy management.

C. BENCHMARK ANALYSIS

In this section, an optimization analysis is presented to demonstrate the efficiency of the proposed algorithm. To achieve this, various mathematical benchmark functions are considered and compared with different metaheuristic algorithms. The CEC 2020 competition test bed [37] is utilized, which consists of 10 benchmark functions with 20 dimensions. The numerical results are presented in Table 5, showcasing the best, worst, median, mean, and standard deviation (SD) values. The evaluated errors are

calculated as $f(x)$-$f(x^*)$, where x represents the best solution and x^* denotes the global optimum value.

Moreover, to further illustrate the efficiency of the proposed algorithm, Table 6 presents the results of the Wilcoxon signed-rank test ($\alpha = 0.05$) for comparisons with other well-known optimization algorithms, including the genetic algorithm (GA) [38], the classic version of PSO, the artificial bee colony (ABC) [39], and the gravitational search algorithm (GSA) [40].

According to Table 6, the sum of ranks for the functions is denoted by R^+ and the sum of ranks for the opposing algorithms is denoted by R^-. Based on the results in the table, it can be confidently asserted that the proposed algorithm surpasses all other optimization algorithms in terms of performance and effectiveness.

V. CONCLUSION

A crucial concern in optimal load planning in energy systems was discussed and addressed in this study. An optimum load flow model based on the enhanced locust search algorithm was proposed for the energy management of community energy hubs. The model incorporated various energy generation resources, EVs, and analyzed the uncertainties using Monte Carlo simulation. The results demonstrated the effectiveness of coordinated charge/discharge modes for EVs and the cost-saving potential of DR programs. Simulation results revealed that the coordinated charge/discharge mode of EV is effective, and cooperative charging/discharging strategy of an EV is able to save the overall costs for 12% as compared to uncoordinated charging approach. The results additionally show a 5% overall cost reduction once DR program was implemented. The proposed strategy provided valuable insights into demand transmission in community energy hubs with high EV penetration. In this process, the improved version of the PSO algorithm was utilized as a solution model for resolving the presented optimization problem. The proposed strategy provides a new insight into the demand transmission of community energy hubs with a high penetration of EVs.

REFERENCES

[1] M. Shafiei and A. Ghasemi-Marzbali, "Electric vehicle fast charging station design by considering probabilistic model of renewable energy source and demand response," *Energy*, vol. 267, Mar. 2023, Art. no. 126545.

[2] O. Abedinia, M. Lu, and M. Bagheri, "An improved multicriteria optimization method for solving the electric vehicles planning issue in smart grids via green energy sources," *IEEE Access*, vol. 8, pp. 3465–3481, 2020.

[3] Z. Feng, X. Lin, Z. Wang, Q. Sui, S. Xu, Z. Li, and C. Wu, "Design and dispatching of all-clean energy producing-consuming system with six-energy coupling," *Int. J. Electr. Power Energy Syst.*, vol. 129, Jul. 2021, Art. no. 106801.

[4] S. Huang and O. Abedinia, "Investigation in economic analysis of microgrids based on renewable energy uncertainty and demand response in the electricity market," *Energy*, vol. 225, Jun. 2021, Art. no. 120247.

[5] X. Lu, Z. Liu, L. Ma, L. Wang, K. Zhou, and N. Feng, "A robust optimization approach for optimal load dispatch of community energy hub," *Appl. Energy*, vol. 259, Feb. 2020, Art. no. 114195.

[6] A. Ghasemi-Marzbali, M. Shafiei, and R. Ahmadiahangar, "Day-ahead economical planning of multi-vector energy district considering demand response program," *Appl. Energy*, vol. 332, Feb. 2023, Art. no. 120351.

[7] M. Bagheri, V. Nurmanova, O. Abedinia, and M. S. Naderi, "Enhancing power quality in microgrids with a new online control strategy for DSTATCOM using reinforcement learning algorithm," *IEEE Access*, vol. 6, pp. 38986–38996, 2018.

[8] H. Khani, A. Sawas, and H. E. Z. Farag, "An estimation–based optimal scheduling model for settable renewable penetration level in energy hubs," *Electr. Power Syst. Res.*, vol. 196, Jul. 2021, Art. no. 107230.

[9] Z. Chen, Y. Zhang, W. Tang, X. Lin, and Q. Li, "Generic modelling and optimal day-ahead dispatch of micro-energy system considering the price-based integrated demand response," *Energy*, vol. 176, pp. 171–183, Jun. 2019.

[10] Q. Lu, S. Lü, Y. Leng, and Z. Zhang, "Optimal household energy management based on smart residential energy hub considering uncertain behaviors," *Energy*, vol. 195, Mar. 2020, Art. no. 117052.

[11] B. Mukhopadhyay and D. Das, "Multi-objective dynamic and static reconfiguration with optimized allocation of PV-DG and battery energy storage system," *Renew. Sustain. Energy Rev.*, vol. 124, May 2020, Art. no. 109777.

[12] J. J. Roberts, A. M. Cassula, J. L. Silveira, E. da Costa Bortoni, and A. Z. Mendiburu, "Robust multi-objective optimization of a renewable based hybrid power system," *Appl. Energy*, vol. 223, pp. 52–68, Aug. 2018.

[13] A. T. D. Perera, V. M. Nik, D. Mauree, and J.-L. Scartezzini, "An integrated approach to design site specific distributed electrical hubs combining optimization, multi-criterion assessment and decision making," *Energy*, vol. 134, pp. 103–120, Sep. 2017.

[14] Y. Jia, Z. Mi, W. Zhang, and L. Liu, "Optimal operation of multi-energy systems in distributed energy network considering energy storage," in *Proc. IEEE Conf. Energy Internet Energy Syst. Integr. (EI)*, Nov. 2017, pp. 1–6.

[15] M. K. Kiptoo, M. E. Lotfy, O. B. Adewuyi, A. Conteh, A. M. Howlader, and T. Senjyu, "Integrated approach for optimal techno-economic planning for high renewable energy-based isolated microgrid considering cost of energy storage and demand response strategies," *Energy Convers. Manage.*, vol. 215, Jul. 2020, Art. no. 112917.

[16] F. Moazeni and J. Khazaei, "Dynamic economic dispatch of islanded water-energy microgrids with smart building thermal energy management system," *Appl. Energy*, vol. 276, Oct. 2020, Art. no. 115422.

[17] V. P. Sakthivel, M. Suman, and P. D. Sathya, "Combined economic and emission power dispatch problems through multi-objective squirrel search algorithm," *Appl. Soft Comput.*, vol. 100, Mar. 2021, Art. no. 106950.

[18] M. A. Bagherian and K. Mehranzamir, "A comprehensive review on renewable energy integration for combined heat and power production," *Energy Convers. Manage.*, vol. 224, Nov. 2020, Art. no. 113454.

[19] D. Huo, S. Le Blond, C. Gu, W. Wei, and D. Yu, "Optimal operation of interconnected energy hubs by using decomposed hybrid particle swarm and interior-point approach," *Int. J. Electr. Power Energy Syst.*, vol. 95, pp. 36–46, Feb. 2018.

[20] F. Brahman, M. Honarmand, and S. Jadid, "Optimal electrical and thermal energy management of a residential energy hub, integrating demand response and energy storage system," *Energy Buildings*, vol. 90, pp. 65–75, Mar. 2015.

[21] B. El-sobky and Y. Abo-Elnaga, "Multi-objective economic emission load dispatch problem with trust-region strategy," *Electr. Power Syst. Res.*, vol. 108, pp. 254–259, Mar. 2014.

[22] H. Ma, Z. Yang, P. You, and M. Fei, "Multi-objective biogeography-based optimization for dynamic economic emission load dispatch considering plug-in electric vehicles charging," *Energy*, vol. 135, pp. 101–111, Sep. 2017.

[23] H. Yang, P. You, and C. Shang, "Distributed planning of electricity and natural gas networks and energy hubs," *Appl. Energy*, vol. 282, Jan. 2021, Art. no. 116090.

[24] M. Geidl, G. Koeppel, P. Favre-Perrod, B. Klockl, G. Andersson, and K. Frohlich, "Energy hubs for the future," *IEEE Power Energy Mag.*, vol. 5, no. 1, pp. 24–30, Jan. 2007.

[25] X. Lu, K. Zhou, S. Yang, and H. Liu, "Multi-objective optimal load dispatch of microgrid with stochastic access of electric vehicles," *J. Cleaner Prod.*, vol. 195, pp. 187–199, Sep. 2018.

[26] M. Mohiti, H. Monsef, and H. Lesani, "A decentralized robust model for coordinated operation of smart distribution network and electric vehicle aggregators," *Int. J. Electr. Power Energy Syst.*, vol. 104, pp. 853–867, Jan. 2019.

[27] Y. Duan, X. He, and Y. Zhao, "Distributed algorithm based on consensus control strategy for dynamic economic dispatch problem," *Int. J. Electr. Power Energy Syst.*, vol. 129, Jul. 2021, Art. no. 106833.
[28] H. Wu, X. Liu, and M. Ding, "Dynamic economic dispatch of a microgrid: Mathematical models and solution algorithm," *Int. J. Electr. Power Energy Syst.*, vol. 63, pp. 336–346, Dec. 2014.
[29] M. J. Vahid-Pakdel, S. Nojavan, B. Mohammadi-Ivatloo, and K. Zare, "Stochastic optimization of energy hub operation with consideration of thermal energy market and demand response," *Energy Convers. Manage.*, vol. 145, pp. 117–128, Aug. 2017.
[30] J. Hu, S. You, M. Lind, and J. Østergaard, "Coordinated charging of electric vehicles for congestion prevention in the distribution grid," *IEEE Trans. Smart Grid*, vol. 5, no. 2, pp. 703–711, Mar. 2014.
[31] G. Li, Y. Li, H. Chen, and W. Deng, "Fractional-order controller for course-keeping of underactuated surface vessels based on frequency domain specification and improved particle swarm optimization algorithm," *Appl. Sci.*, vol. 12, no. 6, p. 3139, Mar. 2022.
[32] Y. Diao, H. Ma, H. Wang, J. Wang, S. Li, X. Li, J. Pan, and Q. Qiu, "Optimal flood-control operation of cascade reservoirs using an improved particle swarm optimization algorithm," *Water*, vol. 14, no. 8, p. 1239, Apr. 2022.
[33] I. U. Rahman, M. Zakarya, M. Raza, and R. Khan, "An n-state switching PSO algorithm for scalable optimization," *Soft Comput.*, vol. 24, no. 15, pp. 11297–11314, Aug. 2020.
[34] W. Deng, J. Xu, H. Zhao, and Y. Song, "A novel gate resource allocation method using improved PSO-based QEA," *IEEE Trans. Intell. Transp. Syst.*, vol. 23, no. 3, pp. 1737–1745, Mar. 2022.
[35] A. Maroufmashat, A. Elkamel, M. Fowler, S. Sattari, R. Roshandel, A. Hajimiragha, S. Walker, and E. Entchev, "Modeling and optimization of a network of energy hubs to improve economic and emission considerations," *Energy*, vol. 93, pp. 2546–2558, Dec. 2015.
[36] G. Han, Y. Xia, and W. Min, "Micro-grid environmental economic dispatch using improved linearly decreasing weight particle swarm optimization," in *Mechatronics and Automatic Control Systems*. Switzerland: Springer, 2014, pp. 491–500.
[37] A. W. Mohamed, A. A. Hadi, A. K. Mohamed, and N. H. Awad, "Evaluating the performance of adaptive GainingSharing knowledge based algorithm on CEC 2020 benchmark problems," in *Proc. IEEE Congr. Evol. Comput. (CEC)*, Jul. 2020, pp. 1–8.
[38] W. Deng, X. Zhang, Y. Zhou, Y. Liu, X. Zhou, H. Chen, and H. Zhao, "An enhanced fast non-dominated solution sorting genetic algorithm for multi-objective problems," *Inf. Sci.*, vol. 585, pp. 441–453, Mar. 2022.
[39] G. Yavuz, B. Durmuş, and D. Aydın, "Artificial bee colony algorithm with distant savants for constrained optimization," *Appl. Soft Comput.*, vol. 116, Feb. 2022, Art. no. 108343.
[40] H. Mittal, A. Tripathi, A. C. Pandey, and R. Pal, "Gravitational search algorithm: A comprehensive analysis of recent variants," *Multimedia Tools Appl.*, vol. 80, no. 5, pp. 7581–7608, Feb. 2021.

OVEIS ABEDINIA (Senior Member, IEEE) received the B.S., M.Sc., and Ph.D. (Hons.) degrees in electrical engineering. He was a Postdoctoral Researcher and a part-time Faculty Member with the Budapest University of Technology, Budapest, Hungary, in 2015, and subsequently started constructing various solar power plants, in 2017. He then, joined Ardabil Science and Technology Park, as the Head of the International Relations. From 2019 to 2023, he successfully oversaw the construction of over 250 solar power plants, varying in size from small to large scale. Since 2019, he has been with Nazarbayev University, as a Research Fellow. He has published over 120 articles and books in various high-ranking journals and conferences. His research interests include power system operations and forecasting. He serves as an editor for several international journals.

AFSHAR SHORKI received the B.Sc. degree from the Department of Mechanical Engineering, University of Mohaghegh Ardabili (UMA), Ardabil, Iran, in 2014, and the M.Sc. degree (Hons.) in energy conversion engineering from the Iran University of Science and Technology (IUST), Tehran, Iran, in February 2017. He is currently pursuing the Ph.D. degree with the University of Tabriz. In his M.Sc., he was involved on Fabrication and Modeling of Solid Oxide Fuel Cell. He is a Scientist, a Research Assistant, and a Research Associate of mechanical engineering. He is also a Research Assistant of energy and environment field working on "optimization and multi-criteria analysis of a multi-generation system based on solid oxide fuel cell". He has published many international journal and conference papers. He is reviewer of several international journals.

VENERA NURMANOVA received the B.Eng. and M.Sc. degrees in electrical and electronic engineering and the Ph.D. degree in science, engineering and technology from Nazarbayev University, Astana, Kazakhstan, in 2015, 2017, and 2022, respectively. She was a Manufacturing Engineer with Granit-Thales Electronics LLP, Almaty, Kazakhstan, in 2017. She is currently a Postdoctoral Researcher with the School of Engineering and Digital Sciences, Nazarbayev University. Her research interests include power systems, high voltage, transformer diagnostics, machine learning, and renewable energy sources.

MEHDI BAGHERI (Senior Member, IEEE) received the Ph.D. degree in electrical power engineering and energy systems from the University of New South Wales (UNSW), Sydney, Australia, in 2014.

He was with the Electric Machinery and Drive Laboratory, Electrical Engineering Department, National University of Singapore (NUS), and closely involved with the Rolls-Royce Pte., Ltd., on a joint project. Since 2016, he has been with Nazarbayev University, where he is currently an Associate Professor with the Department of Electrical and Computer Engineering. He is the Head of the Smart Energy Systems Laboratory. He is actively involved in the advanced testing of industrial projects, and he provides technical support to multinational companies, specializing in power product manufacturing, strategic relationships between industry and academia, energy management, smart monitoring of power equipment, and analysis and development of sustainable energy systems. His research interests include high voltage engineering, wireless power transfer, condition monitoring and assessment, diagnosis of power equipment in the field, space, marine applications, electrical rotating machines, electrical insulation, power quality, and smart energy systems.

Dr. Bagheri was a member of the National Research Council of Kazakhstan, from 2020 to 2023. He is a member of IEEE PES, IES, and DEIS. In recognition of his contributions to engineering, he received the Scopus Award, in 2022. He is an Associate Editor of IEEE Access and the *Frontiers in Energy Research*.